10-18-2018

Evidence That a Respiratory Shield in *Escherichia coli* Protects a Low-Molecular-Mass Fe^{II} Pool from O_2-Dependent Oxidation

Joshua D. Wofford
Texas A&M University

Naimah Bolaji
University of South Carolina - Columbia

Nathaniel Dziuba
Texas A&M University

Franklin Wayne Outten
University of South Carolina - Columbia, outtenf@mailbox.sc.edu

Paul A. Lindahl
Texas A&M University

Publication Info

Published in *Journal of Biological Chemistry*, Volume 294, Issue 1, 2018, pages 50-62.

Evidence that a respiratory shield in *Escherichia coli* protects a low-molecular-mass Fe^{II} pool from O_2-dependent oxidation

Received for publication, August 6, 2018, and in revised form, October 16, 2018 Published, Papers in Press, October 18, 2018, DOI 10.1074/jbc.RA118.005233

Joshua D. Wofford[‡], Naimah Bolaji[§], Nathaniel Dziuba[¶], F. Wayne Outten[§], and Paul A. Lindahl[‡¶1]

From the Departments of [‡]Chemistry and [¶]Biochemistry and Biophysics, Texas A&M University, College Station, Texas 77843 and the [§]Department of Chemistry and Biochemistry, University of South Carolina, Columbia, South Carolina 29208

Edited by Ruma Banerjee

Iron is critical for virtually all organisms, yet major questions remain regarding the systems-level understanding of iron in whole cells. Here, we obtained Mössbauer and EPR spectra of *Escherichia coli* cells prepared under different nutrient iron concentrations, carbon sources, growth phases, and O_2 concentrations to better understand their global iron content. We investigated WT cells and those lacking Fur, FtnA, Bfr, and Dps proteins. The coarse-grain iron content of exponentially growing cells consisted of iron–sulfur clusters, variable amounts of nonheme high-spin Fe^{II} species, and an unassigned residual quadrupole doublet. The iron in stationary-phase cells was dominated by magnetically ordered Fe^{III} ions due to oxyhydroxide nanoparticles. Analysis of cytosolic extracts by size-exclusion chromatography detected by an online inductively coupled plasma mass spectrometer revealed a low-molecular-mass (LMM) Fe^{II} pool consisting of two iron complexes with masses of ~500 (major) and ~1300 (minor) Da. They appeared to be high-spin Fe^{II} species with mostly oxygen donor ligands, perhaps a few nitrogen donors, and probably no sulfur donors. Surprisingly, the iron content of *E. coli* and its reactivity with O_2 were remarkably similar to those of mitochondria. In both cases, a "respiratory shield" composed of membrane-bound iron-rich respiratory complexes may protect the LMM Fe^{II} pool from reacting with O_2. When exponentially growing cells transition to stationary phase, the shield deactivates as metabolic activity declines. Given the universality of oxidative phosphorylation in aerobic biology, the iron content and respiratory shield in other aerobic prokaryotes might be similar to those of *E. coli* and mitochondria.

Iron is critical for virtually all living systems, including *Escherichia coli*, the most extensively studied single-celled organism on the planet (1). This redox-active transition metal is at the active site of numerous enzymes, including respiratory complexes that contain iron–sulfur clusters (ISCs)[2] and heme centers (2, 3). Mononuclear Fe^{II} complexes are particularly dangerous to cells because they react with O_2 or O_2-derived species (*e.g.* H_2O_2) to generate reactive oxygen species (ROS) such as hydroxyl radicals. Regulating iron traffic is critical to minimizing the dangers of this metal in aerobic organisms (4).

The iron content of whole *E. coli* cells has been studied sporadically over the past 4 decades by Mössbauer (MB) spectroscopy, in which transitions from the $I = ½$ ground state of an ^{57}Fe nucleus are induced to the $I = ³⁄₂$ excited state using γ radiation (5, 6). The energies of these transitions are sensitive to the *type* of iron center (ISCs, hemes, nonhemes, etc.) as well as to oxidation state, spin state, and ligand environment. The technique can decompose the major iron-containing species in whole cells and in organelles such as mitochondria into *groups* of iron centers. This partial or *coarse-grain* resolution is better than can be achieved by any other iron-sensitive spectroscopy; however, MB spectroscopy cannot resolve individual iron species. The inherent spectral intensity of each iron in a sample is approximately the same, such that spectral percentages of a center can be converted into absolute iron concentration if the overall iron concentration of the sample is known (*e.g.* as determined by ICP-MS). The most typical spectral feature, called a quadrupole doublet, consists of two equal-intensity lines extending down from the baseline. In a magnetic field, a six-line *sextet* is generally observed. In cases where unpaired electrons generate an internal magnetic field, the sextet "collapses" into a doublet at sufficiently high temperatures.

For magnetically ordered materials, such as the Fe^{III} cores of ferritins, the critical temperature for a related phenomenon is called the blocking temperature (T_B) (7). At temperatures below T_B, magnetically ordered Fe^{III} exhibits a magnetic spectrum, whereas above T_B, this form of iron exhibits a broad quadrupole doublet. *E. coli* cells contain three types of ferritins that store iron under iron-replete conditions. These include ferritin (FtnA), bacterioferritin (Bfr), and miniferritin (Dps) (8). The main iron storage protein is FtnA, a 24-subunit multimer that can bind thousands of iron ions as inert ferric aggregates. Expression of FtnA and Bfr increases dramatically as cells transition from exponential growth to stationary phase (9).

This work was supported by National Institutes of Health Grants R35 GM127021 (to P. A. L.) and R01 GM112919 (to F. W. O.) and Robert A. Welch Foundation Grant A1170 (to P. A. L.). The authors declare that they have no conflicts of interest with the contents of this article. The content is solely the responsibility of the authors and does not necessarily represent the official views of the National Institutes of Health or the Welch Foundation.
This article was selected as one of our Editors' Picks.
This article contains Table S1 and Figs. S1–S7.

[1] To whom correspondence should be addressed: Dept. of Chemistry, Texas A&M University, College Station, TX 77843-3255. Tel.: 979-845-0956; Fax: 979-845-4719; E-mail: lindahl@chem.tamu.edu.

[2] The abbreviations used are: ISC, iron–sulfur cluster; FTS, flow-through solution; LC-ICP-MS, liquid chromatography with on-line detection by an inductively coupled plasma mass spectrometer; LIP, labile iron pool; LMM, low-molecular-mass; MB, Mössbauer; NHHS, nonheme high-spin; OXPHOS, oxidative phosphorylation; ROS, reactive oxygen species; T_B, blocking temperature; T, tesla.

In 1980, Bauminger *et al.* (10) reported that MB spectra of *E. coli* are dominated by a broad quadrupole doublet characteristic of magnetically ordered Fe^{III} ions. Matzanke *et al.* (11) identified a second doublet, representing up to half of the spectral intensity, with parameters typical of nonheme high-spin (NHHS) Fe^{II} complexes coordinated by oxygen and nitrogen ligands. Hudson *et al.* (12) recognized that the Fe^{II} doublet was composed of two subcomponents.

FtnA has a T_B of ~20 K, which is substantially higher than that of the magnetically ordered Fe^{III} species in *E. coli* cells (<3.5 K). Because of this, Bauminger *et al.* (10) suggested that ferritin was *not* the source of the observed magnetically ordered iron. In contrast, Abdul-Tehrani *et al.* (13) concluded that the magnetically ordered iron arose from FtnA.

Iron regulation and metallation of metalloproteins in *E. coli* involve a poorly characterized labile iron pool (LIP) (14–16). The LIP is presumably composed of one or more low-molecular-mass (LMM) nonproteinaceous Fe^{II} complexes in the cytosol. Estimates of the LIP concentration in aerobic bacteria are variable; 1 μM (17), 10 μM (18, 19), 26 μM (20), 15–30 μM (21), and 140 μM (22) have been reported. The size of the LIP increases (to ~177 μM) under anaerobic conditions (20) and reportedly with increasing iron levels in the growth medium (23).

The Fur (ferric uptake regulator) system regulates cellular iron by binding Fe^{II} ions from the LIP and regulating transcription of more than 100 genes involved in iron import, trafficking, and storage as well as in iron-dependent enzyme catalysis and cellular metabolism (24). Fur also controls expression of proteins involved in the TCA cycle and respiration via a small RNA RyhB (25). Fur expression is induced during oxidative stress, which represses iron uptake and limits Fenton chemistry. Δ*fur* cells reportedly contain less iron than WT cells and a higher LIP (13, 18, 21). Δ*fur* cells cannot respire effectively because they are deficient in many iron-containing proteins (25, 27).

Aqueous Fe^{II} ions bind Fur with a K_D of ~1 μM (17, 23, 28) or ~10 μM (19) for one-iron binding and K_{D1} = 30 μM and K_{D2} = 280 μM for two-iron binding (22). Weakly coordinated ligands in the LIP undergo fast ligand exchange, making such complexes difficult to isolate and study. Böhnke and Matzanke (15) isolated and characterized a soluble nonproteinaceous negatively charged iron species from *E. coli* extracts that accounted for 40% of the cellular LIP; they reported a mass of ~2.2 kDa.

Using MB spectroscopy, Abdul-Tehrani *et al.* (13) estimated the concentration of the Fe^{II} species in the cell at ~200 μM, higher than most other estimates and higher than implied by the Fe^{II}-Fur dissociation constant. To explain this, they proposed that the Fe^{II} species observed by MB represented a different pool than is used to bind Fur.

Under aerobic conditions, the LIP is thought to enter cells via any of a number of ferric or ferrous iron transport systems that are largely regulated by Fur. Ferric ions, brought into the cell by siderophore transport systems, are likely reduced to Fe^{II} prior to entry into the cytosolic LIP. Under anaerobic conditions, the *feo* ferrous ion transport system dominates iron import, leading to an increased LIP (20, 29). FNR is an O_2-sensing transcription factor that regulates the shift between aerobic and anaerobic metabolism by regulating >300 genes (30). In the absence of O_2, FNR increases expression of the *feo* iron uptake operon to increase cellular Fe^{II} (20).

Using MB spectroscopy, Hristova *et al.* (31) reported a fourth quadrupole doublet in whole *E. coli* cells, representing ~60% of spectral intensity in their samples. This doublet was attributed to $[Fe_4S_4]^{2+}$ and $[Fe_2S_2]^{2+}$ clusters, low-spin Fe^{II} hemes, and possibly fast-relaxing high-spin Fe^{III} species. Beilschmidt *et al.* (32) assigned the same doublet exclusively to ISCs.

In summary, previous MB studies have decomposed the iron content of *E. coli* into four major groups. These include magnetically ordered Fe^{III} (which may represent the iron core of the ferritin FtnA), two nonheme high-spin Fe^{II} species (some of which may represent the LIP), and a group of overlapping iron centers that include $[Fe_4S_4]^{2+}$ and $[Fe_2S_2]^{2+}$ clusters, low-spin Fe^{II} hemes, and possibly fast-relaxing high-spin Fe^{III} species.

In this study, we used MB spectroscopy (and EPR) to reinvestigate the iron content of *E. coli*. We show that the dominant magnetically ordered Fe^{III} doublet does not arise from ferritins. We use an anaerobic LC-ISC-MS system to detect and partially characterize the LMM Fe^{II} species that may constitute the LIP in these cells. We report a dramatic change in the size of the LMM Fe^{II} pool due to oxygenation state of the growth medium. Our results suggest a major reinterpretation of iron homeostasis in this organism, and they reveal an unexpected and intriguing connection to the iron content of mitochondria and other prokaryotes.

Results

Initial objective: To better understand the iron content of WT E. coli

Although the iron content of *E. coli* has been investigated sporadically using MB spectroscopy over the past 4 decades, many fundamental issues remain unresolved. Most previous studies were focused on the MB of *E. coli* strains in which an iron-containing protein of interest was overexpressed; WT cells served only as the controls. Here, we focused on WT *E. coli*, with mutant strains assisting in that investigation. The word *content* not only refers to the *concentration* of iron in such cells but to a semiquantitative description of the major iron species contained therein. ^{57}Fe-enriched cells were grown on minimal medium using two different carbon sources, three different nutrient iron concentrations, and variable levels of O_2 exposure. Some batches were harvested during exponential growth, whereas others were harvested in stationary phase. Our motivation was to gain a foundational understanding of iron trafficking and regulation in WT *E. coli*, as our previous MB investigations of whole cells have focused on eukaryotic systems. These studies were only performed using minimal medium, and we are uncertain whether results would differ using other growth media.

Exponentially growing E. coli cells contain 400–1600 μM iron, depending on conditions

The iron concentration of *E. coli* cells grown on glucose minimal medium and harvested under exponential growth conditions increased with increasing iron concentration in the growth medium. Cells grown in media supplemented with 1, 10, and 100 μM $^{57}Fe^{III}$ citrate contained 350 ± 120 (n = 4),

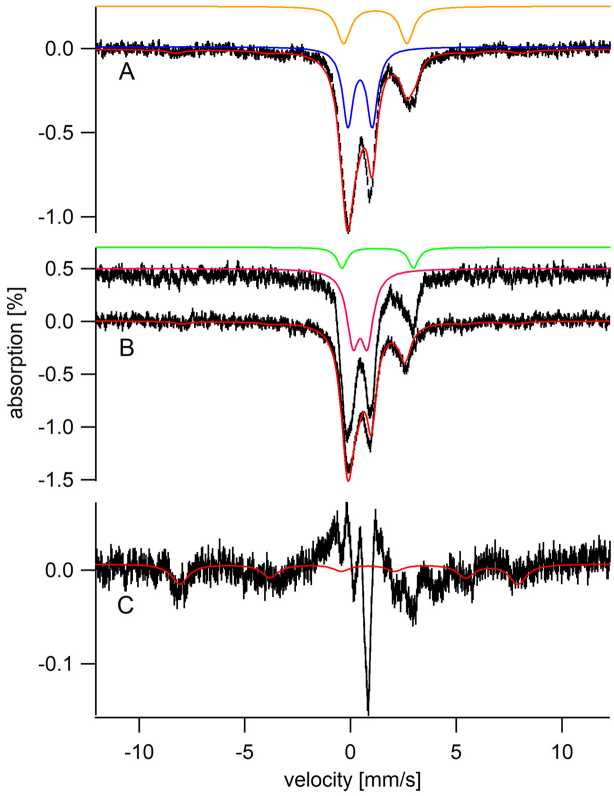

Figure 1. Low-temperature low-field (5 K, 0.05 T) Mössbauer spectra of WT *E. coli* harvested during exponential growth. *A*, glucose medium supplemented with 100 μM $^{57}Fe^{III}$ citrate; *B*, acetate medium supplemented with 1 (*top*) and 100 μM $^{57}Fe^{III}$ citrate (*bottom*). *Gold*, *blue*, *green*, and *pink lines* simulate Fe^{II}_{RET}, ISC, Fe^{II}_{LMM}, and residual doublets, respectively. The *red lines* in this and other figures represent composite simulations assuming components, parameters, and percentages given in Table 1. The presence of the Fe^{II}_{LMM} doublet in the spectrum from acetate-grown cells with 1 μM iron added is evident from the shift in the high-energy line of the NHHS Fe^{II} doublet. The spectrum in *C* is the sum of all six spectra in Fig. 1 and Fig. S1, after removing contributions from the four major doublets. The *red line* in *C* is a simulation assuming parameters typical of $S = 5/2$ Fe^{III} or ferritins (the two cannot be distinguished) with 5% of overall spectral intensity. Unless specified otherwise, the magnetic field was applied parallel to the γ radiation.

540 ± 70 (n = 2), and 990 ± 20 μM iron (n = 2), respectively. WT *E. coli* cells harvested during exponential growth using acetate as the carbon source and in media supplemented with 1, 10, and 100 μM $^{57}Fe^{III}$ citrate contained 600 ± 200 (n = 2), 730 ± 490 (n = 3), and 1600 ± 400 μM iron (n = 2), respectively. These concentrations are ~1.6 times those in glucose-grown cells. See Table S1 for a compilation of other element concentrations. The trends observed were similar to those reported previously (33).

Mössbauer spectra of exponentially growing cells exhibit the ISC and NHHS Fe^{II} doublets, as observed previously, as well as a previously undetected (residual) quadrupole doublet

Low-temperature low-field MB spectra of glucose-grown and exponentially harvested cells were similar regardless of nutrient iron concentration (Fig. 1*A* and Fig. S1, *A* and *B*). The doublet simulated by the *solid blue line* in Fig. 1 and referred to as the *ISC doublet* had parameters (δ = 0.45 mm/s and ΔE_Q = 1.15 mm/s; Table 1) typical of $S = 0$ $[Fe_4S_4]^{2+}$ clusters and low-spin Fe^{II} hemes (the two cannot be resolved by MB). The ISC doublet represented as much as 30% of the overall spectral intensity. The species simulated by the *pink line* in Fig. 1*B* will be referred to as the residual doublet. In some spectra, this doublet represented as much as 40% of the overall intensity (δ = 0.47 mm/s and ΔE_Q = 0.72 mm/s; Table 1). Its isomer shift δ was near to that of $S = 0$ $[Fe_4S_4]^{2+}$ clusters, but the quadrupole splitting ΔE_Q was smaller than normal; thus, we leave this species unassigned. The combined simulation of the ISC and residual doublets, as they would appear at 6 T, was overlaid on the experimental 6 T spectrum in Fig. S2*A*. Although the spectrum was noisy, the fit provides evidence that both ISC and residual doublets arise from diamagnetic $S = 0$ centers, as would be the case for $[Fe_4S_4]^{2+}$ clusters and low-spin Fe^{II} hemes.

Table 1

Components assumed in simulating Mössbauer spectra of *E. coli* and the percentages of each component included in simulations

In addition to the parameters listed for the sextet species, the following parameters were used in simulations: D = 0.5 cm^{-1}, E/D = 0.33, η = 2, $A_{iso}/g_n\beta_n$ = −228 kG.

Mössbauer Component	ISC	Residual	Fe^{II}_{LMM}	Fe^{II}_{RET}	Fe^{III} nanoparticles	S = 5/2 Fe^{III} sextet
δ (mm/s)	0.45 ± 0.01	0.47 ± 0.03	1.33 ± 0.01	1.17 ± 0.05	0.55 ± 0.01	0.54 ± 0.01
ΔE_Q (mm/s)	1.15 ± 0.03	0.72 ± 0.13	3.47 ± 0.01	2.99 ± 0.05	0.55 ± 0.01	0.39 ± 0.01
Γ (mm/s)	0.6 ± 0.1	0.6 ± 0.1	0.6 ± 0.3	0.7 ± 0.1	0.5 ± 0.1	0.4 ± 0.1
Spectrum	%	%	%	%	%	%
Fig. 1A	22	36	07	29	0	05
Fig 1B (top)	28	38	11	18	0	05
Fig. 1B (bot)	31	42	0	34	0	05
Fig. 1C	0	0	0	0	0	05
Fig. 3A	17	0	40	45	0	0
Fig. 3B	11	0	30	54	0	0
Fig. 3C	19	18	37	27	0	0
Fig. 4A	21	7	24	55	0	0
Fig. 4B	18	4	31	51	0	0
Fig. 4C	12	7	31	43	0	0
Fig. 5A	10	29	15	44	0	0
Fig. 5B	13	0	0	10	61	0
Fig. 5C	30	32	09	15	0	10
Fig. 5D	26	39	06	15	0	06
Fig. 5E	13	0	0	10	76	0
Fig. 5F	23	12	35	18	11	0
Fig. 5G	31	15	13	37	0	0
Fig. 7A	17	20	29	21	16	0
Fig. 7B	17	20	16	21	29	0
Fig. 7C	0	0	-13	0	13	0
Fig. 8A	11	31	10	48	0	0
Fig. 8B	0	0	100	0	0	0
Fig. 8C	13	29	32	35	0	0
Fig. 8D	13	29	0	35	0	0

The other major quadrupole doublet of Fig. 1*A* had parameters of NHHS Fe^{II} species coordinated by 4–6 oxygen, 0–2 nitrogen, and few if any sulfur donor ligands. The doublet was broader than expected for one species, so two subcomponents (Fe^{II}_{RET} and Fe^{II}_{LMM}) were assumed (δ = 1.17 mm/s and ΔE_Q = 2.99 mm/s (Fe^{II}_{RET}) and δ = 1.33 mm/s and ΔE_Q = 3.47 mm/s (Fe^{II}_{LMM})). The *green* and *gold lines* in Fig. 1 (*A* and *B*) simulate the two subcomponents (Table 1). The subscripts RET and LMM are explained below.

Acetate-grown and exponentially harvested cells exhibited the MB spectra shown in Fig. 1*B* and Fig. S1 (*C* and *D*). Cells grew less than half as fast on acetate as they did on glucose; the average exponential growth rate α was 0.40 ± 0.04 h^{-1} for glucose-grown cells and 0.17 ± 0.03 h^{-1} for acetate-grown cells (n = 3 for each). *E. coli* converts acetate directly to acetyl-CoA, which is then sent to the TCA cycle without involving glycolysis (34). In contrast, cells first convert glucose to acetyl-CoA via glycolysis (and pyruvate dehydrogenase). Thus, acetate-grown cells respire exclusively, whereas glucose-grown cells both respire and ferment, depending on local oxygen and glucose concentrations.

MB spectra of acetate-grown cells were similar to those grown in glucose, except that the ISC and residual doublets were slightly more intense, consistent with a higher iron concentration. Acetate-grown cells probably contain a higher concentration of iron-rich respiration-related proteins. We also observed a shift in the position of the Fe^{II} doublet, depending on the iron concentration in the growth medium. For the sample grown with 1 μM $^{57}Fe^{III}$ citrate, 11% of spectral intensity was Fe^{II}_{LMM} (Fig. 1*B*, *top spectrum*). For samples grown with 10 or 100 μM $^{57}Fe^{III}$ citrate (Fig. 1*B*, *bottom spectrum*), no Fe^{II}_{LMM} was evident.

Only ~5% of MB intensity could be due to ferritins in exponentially grown cells

We searched for low-intensity features emanating from the baselines associated with the spectra of Fig. 1 and Fig. S1. Such features, if present, might arise from paramagnetic centers, such as $S = 5/2$ Fe^{III} hemes, or from superparamagnetic centers, such as ferritins (at temperatures below their T_B). To probe this, we summed the six spectra and removed the major spectral features described above. The resulting difference spectrum (Fig. 1*C*) exhibited weak spectral absorption, which could be simulated using parameters of either $S = 5/2$ Fe^{III} hemes and nonheme species or of ferritins below their T_B. Magnetic features with $S = 1/2$ may have also been present but obscured by features of the central spectral region. Collectively, these magnetic baseline features constituted ~5% of overall spectral intensity. We include this estimate in the composite simulations of Fig. 1, *A* and *B* (Table 1).

EPR spectra confirm Mössbauer analysis; exponentially grown cells contain minor levels of paramagnetic ISCs and heme centers

Glucose- and acetate-grown whole cells exhibited EPR signals in the low-field (g = 4–6) and high-field (g ~2) regions (Fig. 2). Spectral decomposition identified three low- and three high-field signals (Fig. S3). Low-field signals were typical of $S = 5/2$ hemes and nonheme Fe^{III} species. High-field signals included two $g_{ave} = 1.94$ type signals arising from reduced $S = 1/2$ $[Fe_4S_4]^{1+}$ and/or $[Fe_2S_2]^{1+}$ clusters, as well as an unassigned isotropic g = 2.00 signal. Similar spectra of whole *E. coli* cells have been reported (25) except that signals from $[Fe_3S_4]^{1+}$ centers were not observed in our spectra, and the low-field signals in our reductant-free spectra were more typical of signals of previous dithionite-reduced cells. All current signals except the radical were 2–10 times more intense in acetate-grown cells than in glucose-grown cells (the intensity of the radical was similar in both spectra). The overall spin concentration in the g = 2 region was ~60 μM for the acetate-grown sample and 20 μM for the glucose-grown sample. We did not quantify the signals in the low-field region, but concentrations are likely of the same magnitude or less. We assumed that these paramagnetic centers contributed <5% to the central regions of the MB spectra and a similar percentage in the "wings." This makes the EPR signals consistent with the minor intensity associated with paramagnetic centers in the MB of Fig. 1*C*, and it suggests

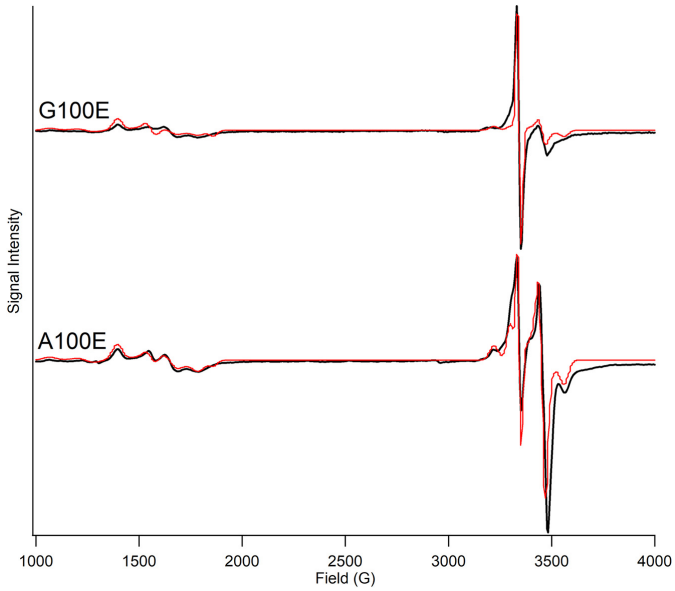

Figure 2. Low-temperature X-band EPR spectra of whole packed *E. coli* cells grown on glucose (G100E) or acetate (A100E) and harvested under exponential growth conditions. Samples were grown in media supplemented with 100 μM Fe^{III} citrate. Composite simulations are the *red lines* overlaying the data (*black lines*). Individual simulations are shown in Fig. S3. Temperature was 10 K, microwave frequency was 9.38 GHz, microwave power was 0.2 milliwatt, time constant was 0.293 s, and modulation amplitude was 10 G.

that most ISCs in WT *E. coli* cells are diamagnetic and oxidized (*i.e.* $[Fe_4S_4]^{2+}$ and $[Fe_2S_2]^{2+}$ clusters).

The intensity of the NHHS Fe^{II} doublets was correlated to O_2 levels during growth

In some spectra, the NHHS Fe^{II} doublets were significantly more intense than in Fig. 1, reaching as high as 85% of overall intensity for the MB spectra (Fig. 3). This variation was initially puzzling because batches were grown on the same medium, using the same concentration of nutrient $^{57}Fe^{III}$ citrate, and harvested at about the same A_{600}. Like Beauchene *et al.* (20), we discovered that the concentration of NHHS Fe^{II} in cells was affected by the O_2 concentration in the culture. Subtle changes in aerobicity (*e.g.* caused by differences in rotation rates of the shaker or in volume ratios of liquid culture to flask capacity) affected the intensity of the Fe^{II} spectral features. *Higher* concentrations of NHHS Fe^{II} species correlate with *lower* O_2 concentrations.

Δfur cells have dysregulated Fe$^{II}_{LMM}$

We were surprised that modest changes in O_2 had a significant effect on the concentration of NHHS Fe^{II} in WT cells; we had expected that Fe^{II} concentrations would be tightly regulated by Fur. To investigate further, Δ*fur* cells were grown on glucose media supplemented with 1, 10, and 100 μM $^{57}Fe^{III}$ citrate. Like WT cells, Δ*fur* cells exhibited MB spectra dominated by NHHS Fe^{II} and ISC doublets (Fig. 4). Iron concentrations of a different set of Δ*fur* cells but grown in the same way were 420 ± 10, 1460 ± 240, and 4300 ± 70 μM, respectively ($n = 2$ for each). The most significant spectroscopic difference relative to WT was the increased intensity of the Fe^{II}_{LMM} doublet relative to other features as the concentration of nutrient iron increased. This effect was not observed in WT cells; it

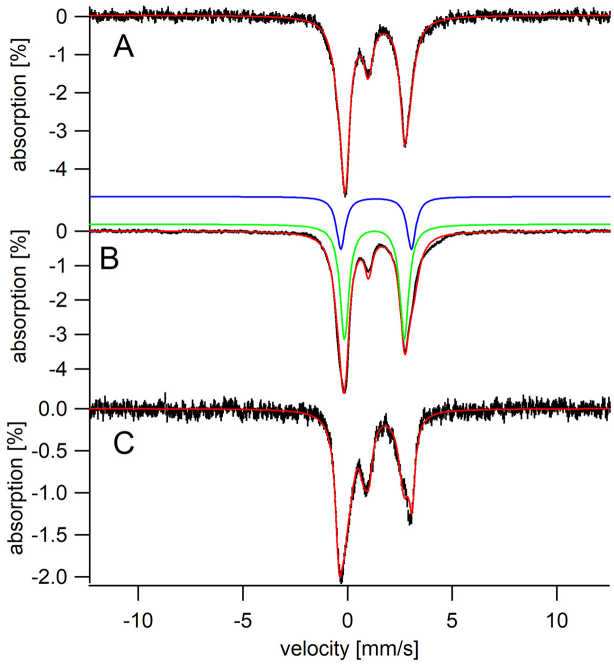

Figure 3. Mössbauer spectra (5 K, 0.05 T) of three separate batches (*A*, *B*, and *C*) of WT *E. coli* cells grown in glucose under reduced O_2 conditions. *Blue* and *green lines*, simulations of the Fe^{II}_{LMM} and Fe^{II}_{RET} species, respectively.

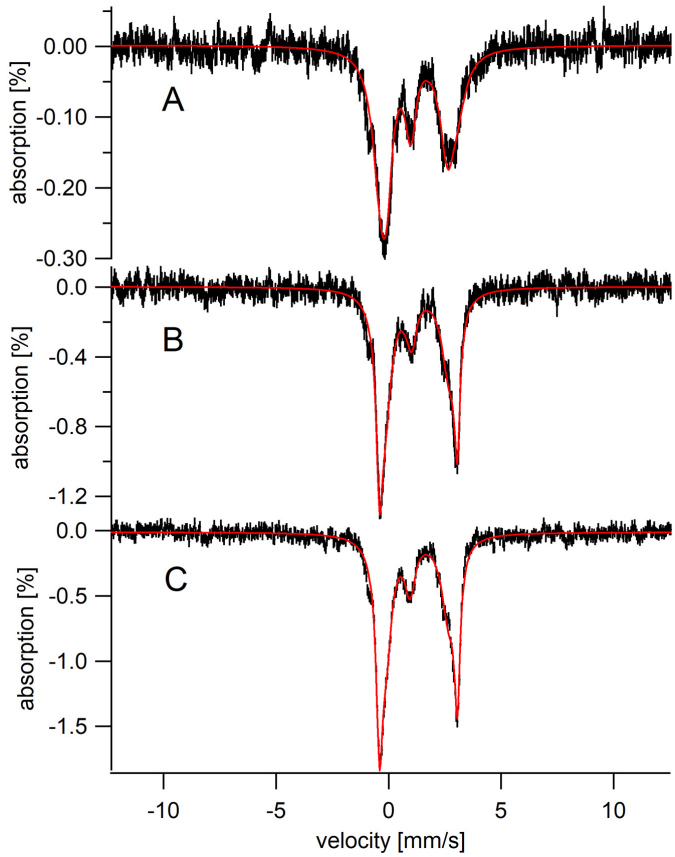

Figure 4. Mössbauer spectra (5 K, 0.05 T) of whole Δ*fur* cells grown on glucose medium and harvested during exponential phase. The concentration of $^{57}Fe^{III}$ citrate was 1 (*A*), 10 (*B*), or 100 μM (*C*).

implies that the species responsible for the Fe^{II}_{LMM} doublet is not well regulated in Δ*fur* cells (13, 18). The presence of higher concentrations of iron in Δ*fur versus* WT cells also implies

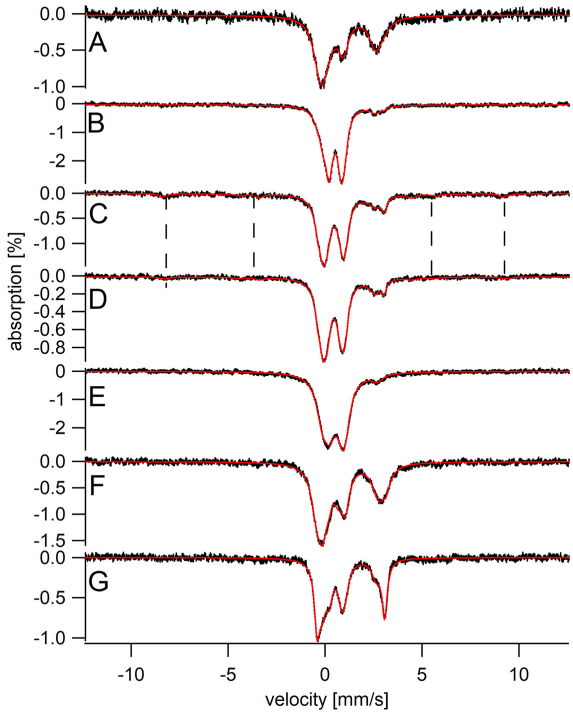

Figure 5. Mössbauer spectra (0.05 T) of whole *E. coli* cells grown on minimal medium, supplemented with 100 μM ^{57}Fe citrate, and harvested during exponential and stationary phases. *A*, WT cells harvested during exponential growth. *B*, same as *A* but harvested in stationary phase. *C*, Δ*ftnA* cells harvested during exponential growth. *D*, same as *C* except collected at 100 K. *E*, same as *C* and *D* except harvested in stationary phase. *Vertical dashed lines* between *C* and *D* highlight the Fe^{III} sextet extending slightly from the baseline. *F*, Δ*bfr*Δ*dps* cells harvested during exponential phase. *G*, same as *F* but harvested during stationary phase. *Spectra A*, *B*, *C*, *E*, *F*, and *G* were collected at 5 K.

poorer regulation in Δ*fur* cells. These results differ from a previous report (13) in which the iron concentration in Δ*fur* cells was *less* than that of WT cells. Perhaps the difference arises because we harvested these cells during exponential phase, whereas Abdul-Tehrani *et al.* (13) harvested them during stationary phase. The mechanism of Fur regulation implies that the concentration of iron in Δ*fur* cells should be higher than in WT cells, as we observed.

Mössbauer spectra of cells harvested at stationary phase were dominated by magnetically ordered Fe^{III}

WT cells harvested in stationary phase exhibited a broad quadrupole doublet with parameters typical of magnetically ordered Fe^{III} (Fig. 5*B*). This doublet was largely absent in spectra of cells harvested during exponential growth (Fig. 5*A*). The Fe^{II} doublets were stronger in spectra from exponentially growing cells, whereas the ISC and residual doublet intensities were almost unchanged regardless of growth phase. This suggests that the species in the cell that gives rise to these latter doublets are less sensitive to the metabolic changes associated with the exponential → stationary shift than are the cell's Fe^{II} species. The overall percentage effect nearly doubled in the MB spectrum of stationary-phase cells relative to that of exponentially growing cells. This implies that stationary-phase cells import iron even when the cells are not growing. We observed a similar phenomenon in yeast (35).

Magnetically ordered Fe^{III} arises from oxyhydroxide nanoparticles rather than ferritins

The magnetically ordered Fe^{III} doublet was similar to that arising from Fe^{III} oxyhydroxide nanoparticles in mitochondria for which ISC assembly is impaired (36) (see Fig. S4*B*). Also, the high-field spectrum of the magnetically-ordered material in *E. coli* (Fig. 5 of Popescu *et al.* 37) was remarkably similar to that of mitochondrial nanoparticles (38, 39). Thus, we assign this spectral feature to Fe^{III} oxyhydroxide nanoparticles.

Some past investigators assigned this feature to iron bound in ferritin cores (8, 15, 36), whereas others doubted such an assignment (10, 11, 32, 39). To settle the issue, we repeated the experiment using three genetic strains of *E. coli* (Δ*ftnA*, Δ*bfr*, and Δ*bfr*Δ*dps*) in which ferritin-related genes were deleted. As above, a portion of a growing culture was harvested during exponential phase, and the remainder was harvested later in stationary phase. In the experiments involving Δ*ftnA* and Δ*bfr*, samples harvested during exponential growth exhibited little if any intensity from the magnetically ordered doublet (see Fig. 5 (*C* and *D*) for Δ*ftnA* and Fig. S5*A* for Δ*bfr*), whereas the corresponding samples harvested during stationary phase were dominated by this material (Fig. 5*E* for Δ*ftnA* and Fig. S5*B* for Δ*bfr*). The iron concentration of Δ*ftnA* cells increased from 1.2 to 2.0 mM as cells transitioned from exponential to stationary phase. The corresponding iron concentration shifts for Δ*bfr* and WT cells were from 1.6 to 1.8 mM and from 1.1 to 1.3 mM, respectively.

The magnetically ordered iron in these spectra could not have originated from the major ferritin or bacterioferritin in *E. coli* because the corresponding genes had been deleted. The Δ*ftnA* 5 K spectral baseline in Fig. 5*C* suggested a hint of magnetic material (~5% of total intensity) in the wings. We collected a spectrum at 100 K and found that about half of the intensity remained, suggesting that no more than ~3% of cellular iron might be due to ferritins. We cannot identify the ferritin-like species that could be involved, but it cannot be FtnA. The EPR spectrum suggests that most of the magnetic material emanating from the baseline arose from high-spin $S = 5/2$ Fe^{III} hemes and nonheme Fe^{III} (see above). In summary, our results indicate that no more than ~3% of cellular iron (~50 μM) could be due to ferritins in any experiment performed in this entire study.

The results of two experiments with the Δ*bfr*Δ*dps* strain differed from those of WT, Δ*ftnA*, or Δ*bfr* cells. In duplicate experiments, the spectra of exponential and stationary phase were similar (Fig. 5 (*F* and *G*) and Fig. S5 (*C* and *D*)); nanoparticles did not form under what was ostensibly stationary phase. However, these cells grew slowly and may not have reached true stationary phase when they were harvested. Also, the iron concentration of Δ*bfr*Δ*dps* cells declined slightly (from 980 to 880 μM) during the exponential → stationary transition, which differed from the other ferritin mutants.

The iron content of E. coli is similar to that of mitochondria

We have studied mitochondria from yeast and human cells extensively using MB and EPR spectroscopies (*e.g.* see Refs. 36, 38, and 40) and were surprised by the remarkable similarity to *E. coli*. MB spectra of *E. coli* cells harvested during exponential state were similar to those of mitochondria isolated from respiring cells (compare Fig. 1 with Fig. S4*A*), whereas MB spectra of *E. coli* cells harvested in stationary phase were similar to those of mitochondria isolated from yeast cells with a defect in ISC assembly (compare Fig. 5 (*B* and *E*) with Fig. S4*B*).

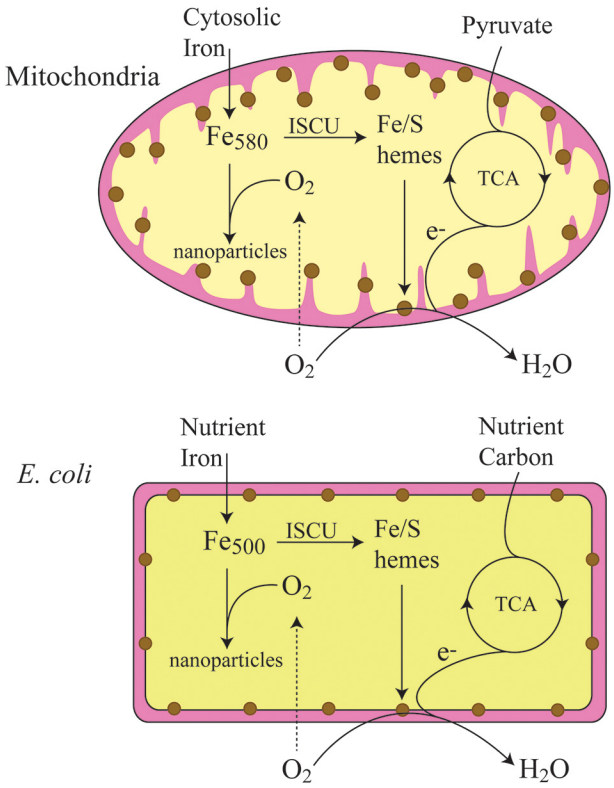

Figure 6. Respiratory shield model for mitochondria (*top*) and *E. coli* (*bottom*). The respiratory shield consists of the ISC- and heme-containing respiratory complexes located in the inner membrane of mitochondria and the cytoplasmic membrane of *E. coli* and other prokaryotes. The shield is operational when cells are metabolically active, oxidizing nutrient carbon and passing electrons through the respiratory electron-transfer chain and reducing some diffusing O_2 to water. With the shield operational, the cytosolic regions become microaerobic. This protects the labile Fe^{II} pool in the cell from reaction with O_2. When cells transition to stationary phase, they become metabolically less active, and the shield deactivates. Then additional O_2 diffuses into the cytosol, where it reacts more rapidly with the labile Fe^{II} pool, forming Fe^{III} oxyhydroxide nanoparticles. A similar deactivation of the shield occurs when respiratory complex IV is inhibited by cyanide.

We have developed a chemical model that explains how nanoparticles form in mitochondria from ISC-defective mutants (41, 42). Accordingly, nanoparticles are generated when a LMM Fe^{II} complex called Fe_{580} reacts with O_2 or a derivative thereof (Fig. 6, *top*). Our model assumes that the matrix of the WT mitochondria is microaerobic under healthy conditions, due to the ability of the iron-rich respiratory complexes on the inner membrane to hinder O_2 from diffusing into the matrix and reacting with Fe_{580}. In ISC-defective mutants, the respiratory complexes are less effective due to incomplete metallation of these complexes. The additional O_2 that diffuses into the matrix of unhealthy mitochondria reacts with Fe_{580} to generate nanoparticles in a vicious cycle.

The similar iron content of *E. coli* and mitochondria suggested a similar explanation for how nanoparticles are generated in this bacterium during stationary phase. We hypothesize

that the cytosol of exponentially growing *E. coli* cells is sufficiently reducing to maintain the Fe^{II} state of a LMM Fe^{II} complex called Fe_{500} (see below) and that this space is sufficiently oxidizing in stationary-phase cells to support O_2-dependent oxidation of $Fe^{II} \rightarrow Fe^{III}$ oxyhydroxide nanoparticles.

For *E. coli* transitioning into stationary phase, the low activity of respiratory complexes is caused, not by insufficient ISC or heme centers, but by low metabolic levels. The flow of electrons through respiratory centers can as readily be restricted by insufficient reducing equivalents as it can by insufficient iron centers. We suggest that the respiratory complexes on the periplasmic membrane of *E. coli* constitute a "shield" that partially blocks O_2 from penetrating the cytosol. This shield, when operational, maintains the cytosol in a microaerobic (although not fully anaerobic) state. When exponentially growing cells transition to stationary phase, metabolic activity declines and the shield deactivates such that the cytosol becomes more oxygenated.

Inhibiting respiratory complex IV with cyanide generates nanoparticles from NHHS Fe^{II} in E. coli, suggesting a protective "respiratory shield" against O_2 or O_2-derived species

To test this hypothesis, we inhibited cytochrome *c* oxidase activity in exponentially growing cells by treating cells with sodium cyanide, a well-known inhibitor of this respiratory complex. Prior to treatment, cells grew rapidly ($\alpha = 0.26\ h^{-1}$), and after treatment, they quickly stopped growing ($\alpha \sim 0\ h^{-1}$). MB samples of each state were prepared. After 90-min incubation, 13% of cellular iron in the form of NHHS Fe^{II} had converted to nanoparticles, as observed in the difference MB spectrum (Fig. 7*C*). The parameters needed to simulate the observed NHHS Fe^{II} doublet were those of Fe^{II}_{LMM}. The other doublet was simulated using parameters typical of nanoparticles (Table 1). That only the Fe^{II}_{LMM} doublet was affected suggests that the iron species giving rise to this doublet is particularly susceptible to oxidation by O_2 or its ROS derivatives. We cannot exclude the possibility that the nanoparticle doublet might include other forms of Fe^{III} that have similar isomer shift and quadrupole splitting parameters; nor can we exclude the possibility that some effects of cyanide treatment may have been due to the binding of cyanide to cellular species other than cytochrome *c* oxidase.

Mössbauer spectra of LMM flow-through solutions and retentate of E. coli soluble extracts distinguish Fe^{II}_{RET} from Fe^{II}_{LMM}

We wondered whether the NHHS Fe^{II} species in *E. coli* that give rise to the Fe^{II}_{RET} and/or Fe^{II}_{LMM} doublets were bound to Fe^{II}-containing proteins or whether they were nonproteinaceous LMM Fe^{II} complexes. Such structural differences would suggest different physiological roles. Small Fe^{II} complexes might be associated with the LIP and function in iron trafficking and regulation, in Fenton chemistry, and as substrates for ISC/heme assembly (13, 18, 20, 21, 27, 43). In contrast, Fe^{II}-containing proteins often serve catalytic roles.

To distinguish the species giving rise to these two Fe^{II} doublets, three MB samples were brought into an anaerobic glove box after their spectra had been collected. The averaged spectrum exhibited a strong NHHS Fe^{II} doublet (Fig. 8*A*), indicating a high concentration of Fe^{II} species. Samples were thawed, diluted with buffer, and lysed. The supernatant was then passed through a 10-kDa cutoff membrane. The retentate and flow-through solutions (FTSs) were collected and transferred to MB cups. The retentate should have contained soluble iron-bound proteins, whereas the FTS should have been largely protein-free. The MB spectrum of the FTS (Fig. 8*B*) exhibited a sharp NHHS Fe^{II} doublet, which was simulated using parameters of the Fe^{II}_{LMM} doublet associated with whole-cell spectra (Table 1). This suggests that Fe^{II}_{LMM} is a LMM Fe^{II} complex that passes through the 10-kDa cutoff membrane (which explains our nomenclature). A MB spectrum of the FTS was also collected at 6 T and 4.2 K (Fig. S2*B*). Although noisy, it could be simulated using a high-spin Fe^{II} Hamiltonian.

The low-field 5 K MB spectrum of the retentate (Fig. 8*C*) also exhibited the Fe^{II}_{LMM} doublet along with other features. The presence of the Fe^{II}_{LMM} doublet in the retentate was expected because we did not wash this solution (*e.g.* by adding buffer and reconcentrating) to remove all traces of LMM Fe^{II}_{LMM}. To highlight the other features in the retentate spectrum, we subtracted the Fe^{II}_{LMM} doublet. The Fe^{II}_{RET} doublet was present in the resulting spectrum (Fig. 8*D*), as was another broad doublet near the central region. This latter doublet was composed of the ISC and residual doublets. The species giving rise to these doublets should be high-molecular-mass and probably proteinaceous, in that protein-bound iron cofactors should be retained by the 10-kDa cutoff membrane.

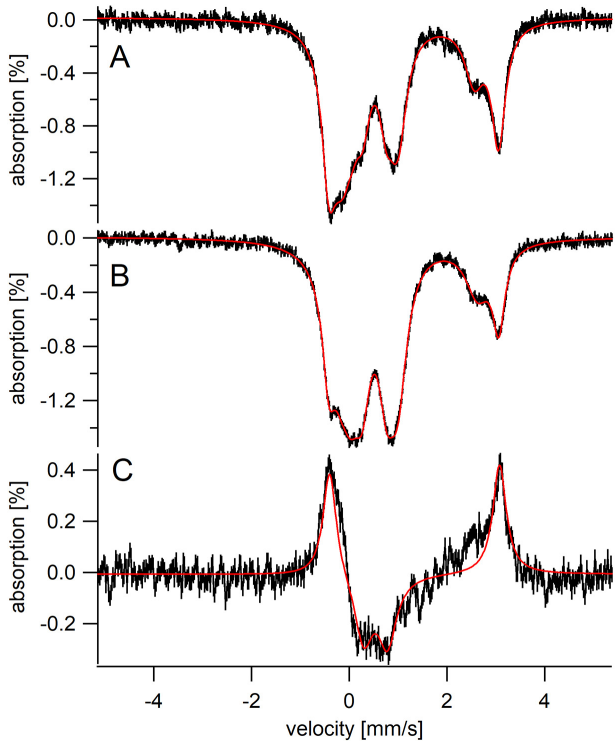

Figure 7. Mössbauer spectra (5 K, 0.05 T) of cyanide-treated *E. coli* cells. *A*, before treatment; *B*, after treatment. *C*, a difference spectrum of *B* − *A*. The *solid red line* in *C* is a simulation in which the Fe^{II}_{LMM} doublet in *A* is replaced by the nanoparticle doublet in *B* (13% of spectral intensity for each).

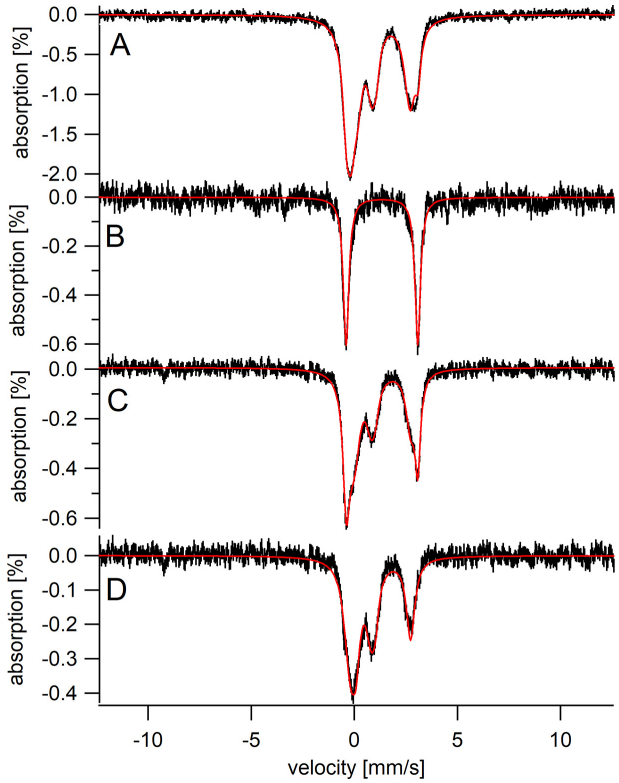

Figure 8. Mössbauer spectra (5 K, 0.05 T) of whole *E. coli* cells and associated retentate and flow-through solutions. *A*, sum of the spectra obtained of the three samples used in the experiment; *B*, FTS; *C*, retentate; *D*, same as *C* except after removing the Fe^{II}_{LMM} contribution.

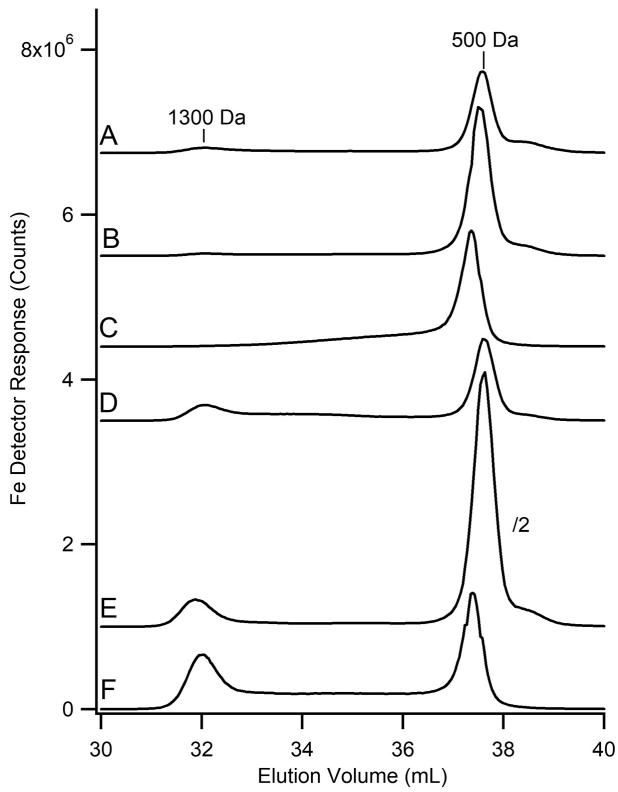

Figure 9. ^{57}Fe-detected LC-ICP-MS chromatograms of flow-through solutions from exponentially grown *E. coli* cells. *Traces A*, *B*, and *C* were for glucose-grown cells in which media were supplemented with 1, 10, and 100 μM $^{57}Fe^{III}$ citrate, respectively. *D*, *E*, and *F*, the same respective iron concentrations for acetate-grown cells.

LC-ICP-MS chromatograms of flow-through solutions reveal that the LIP consists of two iron complexes

In some samples, a portion of the FTS was analyzed for metal concentrations. For one sample, the concentration of LMM iron within the cell was back-calculated from the iron concentration in the FTS. After multiplying by all dilution factors involved in preparing the sample from whole cells, the concentration of LMM iron species within whole cells was calculated to be ~200 μM.

We then used LC in conjunction with an online ICP-MS to detect LMM iron species in soluble *E. coli* extracts. FTSs from such extracts were separated on a size-exclusion column designed to resolve LMM peptides, and the eluent fractions flowed into an online ICP-MS. Iron-detected chromatograms are shown in Fig. 9; those of the other elements are presented in Fig. S6.

One major LMM iron species was detected in all chromatographs, with a mass of ~500 Da (to be referred to as Fe_{500}). A minor LMM iron species at ~1300 Da was evident in all chromatograms but was more intense in FTSs from acetate-grown cells. The intensities of Fe_{500} peaks did not vary systematically with the concentration of nutrient iron in cells grown on glucose, but in acetate-grown cells, Fe_{1300} increased with increasing nutrient iron levels. In one experiment, the cells contained 370 μM iron (at a collective volume of 1.42 ml), whereas the 600 μl of FTS contained 230 μM iron. This suggests that ~26% of total cellular iron was LMM; this compares nicely to the MB percentage of Fe^{II}_{LMM} for this sample, namely 20%. We conclude that Fe_{500} and Fe_{1300} collectively give rise to the Fe^{II}_{LMM} doublet in the MB spectra of *E. coli* cells. We hypothesize that these two LMM species constitute the LIP.

Discussion

Composition and properties of the LMM Fe^{II} pool in E. coli

In this study, we have isolated two LMM Fe^{II} complexes from *E. coli*, which we call Fe_{500} and Fe_{1300} (subscripts indicate approximate masses in Da). Fe_{500} was the major component in all samples investigated. The concentration of Fe_{1300} was variable, with higher levels in samples grown on acetate and under iron-replete conditions. The concentration of this pool depended on the level of O_2 exposure during cell growth. Under more aerobic conditions, the LMM Fe^{II} concentration in WT *E. coli* cells was only ~50 μM, whereas under less aerobic conditions, it exceeded 500 μM in some samples.

Our results suggest that these LMM Fe^{II} complexes are not artifacts of isolation. The δ and ΔE_Q parameters for the Fe^{II}_{LMM} doublet exhibited by isolated FTS were the same as those for MB spectra of intact *E. coli* cells. We generated the FTS from whole cells rapidly in a refrigerated anaerobic glove box to avoid oxidation to the Fe^{III} state and to slow potential ligand-exchange reactions. The intensity of the Fe^{II}_{LMM} doublet in whole cells varied with O_2 levels similar to the effect observed by Kiley and co-workers (20). Also, the FTS Fe^{II} quadrupole doublet was sharper than would be expected for adventitious Fe^{II}, which would generally be broadened due to heterogeneity. Also, the

Table 2
Comparison of Mössbauer parameters associated with the two low-molecular mass NHHS Fe^{II} species observed in spectra of *E. coli* cells to selected Fe^{II} complexes
The numbers of oxygen and nitrogen donor atoms coordinating the complexes are indicated by subscripts.

Fe^{II} Complex	δ (mm/s)	ΔE_Q (mm/s)
Fe^{II}_{LMM}	1.33	3.47
$Fe^{II}(O_6)$ (59)	1.30	3.13
$Fe^{II}(H_2O)_6$ (60)	1.34	3.4
Fe^{II}_{RET}	1.17	2.99
$Fe^{II}(N_3O_3)$ (61)	1.19	3.07
$Fe^{II}(N_4O_1)$ (61)	1.196	3.047
$Fe^{II}(N_4O_2)$ (26)	1.195	3.131

simplicity of the LMM chromatograms, which reproducibly exhibited only peaks from Fe_{500} and Fe_{1300}, is inconsistent with our expectation that adventitious iron would show batch-to-batch variation with multiple irreproducible peaks. Finally, aqueous Fe^{II}/Fe^{III} solutions, which would likely be a component of adventitious iron, adsorb strongly on our columns (44), whereas the LMM iron complexes observed here do not. We hypothesize that the physiological labile iron pool in *E. coli* consists mainly of one NHHS Fe^{II} complex with an approximate mass of 500 Da. A second minor species with a mass of ~1300 Da is also present. The low mass of these complexes suggests that they are not proteins. We do not know the functions of Fe_{500} or Fe_{1300} but speculate that they are involved in iron trafficking, sensing, and/or regulation. They might serve as feedstock for building ISCs and/or hemes or for metallating various apoenzymes. Further studies are required to evaluate these possibilities.

Comparing δ and ΔE_Q parameters for the Fe^{II}_{LMM} doublet with those from chemically defined high-spin Fe^{II} complexes (Table 2) provides some insight into the coordination environment of Fe_{500}. An Fe^{II} ion coordinated to six oxygen donors affords similar parameters. The parameters for Fe^{II}_{RET} are closer to those of Fe^{II} complexes with a mixture of nitrogen/oxygen donor ligands.

A new perspective for iron regulation in E. coli

A popular notion is that only a small portion of cellular iron is present as labile Fe^{II}, only enough for regulatory sensing and trafficking so as to minimize Fenton chemistry (14, 23). Consequently, the LIP is thought to be buffered in the low micromolar range (35, 43, 45). This view is supported by our results for cells grown under aerobic conditions; here, the concentration of the LMM Fe^{II} pool was 50 μM or less. However, the situation is different under microaerobic conditions in which the LMM Fe^{II} concentration can exceed 500 μM. If K_D for binding of Fe^{II} to Fur equals ~1 μM (17, 23, 28), virtually all Fur in these cells should be bound with Fe^{II} under most nutrient iron conditions. How might Fur serve as a regulator under these conditions? One possibility is that the K_D is actually weaker than 1 μM; higher values have been reported (19, 22), including one as high as K_D = 280 μM. There is more than one binding site on Fur; perhaps sites that bind Fe^{II} weakly may be physiologically relevant. Another possibility is that only certain Fe^{II} complexes within the LIP bind Fur, and yet another possibility is that LIP levels in anaerobic/microaerobic cells are not as tightly regulated as is generally assumed.

Beauchene *et al.* (20) suggested that expression of the *feo* genes that control iron import under anaerobic conditions might be controlled more by FNR than by Fur. However, our results suggest that the concentration of Fe^{II}_{LMM} is Fur-dependent. Its concentration in Δ*fur* cells was significantly affected by the concentration of iron in the medium, whereas its concentration in WT cells was not. Without Fur, Fe^{II}_{LMM} does not seem to be well regulated.

A modified role of ferritins in E. coli

Abdul-Tehrani *et al.* (13) concluded from their MB study of iron-replete WT *E. coli* that half of the iron in cells harvested in stationary phase was bound to FtnA ferritin. They assumed that the magnetically ordered Fe^{III} material observed in MB spectra of such cells arose from ferritin iron cores. During exponential growth, the concentration of iron in the cell was about half of what it was at stationary state, due, they suggested, to the absence of the magnetically ordered Fe^{III} (*i.e.* FtnA-bound iron). This conclusion was reasonable because expression of FtnA increases 10-fold as exponentially growing cells transition to stationary phase (13).

In contrast, we found virtually no evidence for iron bound to ferritin in any *E. coli* sample studied, including iron-replete WT samples harvested at stationary state. We observed an intense magnetically ordered Fe^{III} doublet in 5 K MB spectra of stationary-phase cells, and indeed this material represented over half of the iron in those samples. However, this material does not arise from FtnA-bound iron, as evidenced by the following results. First, the same doublet was observed in stationary-state cells lacking FtnA and Bfr. The doublet had δ and ΔE_Q typical of Fe^{III} oxyhydroxide nanoparticles in mitochondria. The T_B of the doublet, like that of mitochondrial nanoparticles, is <5 K. This explains why we observed (in *E. coli* spectra) a broad doublet at 5 K, whereas others observed magnetic interactions for the same material at 1.7 K (13).

Although the baselines of our 5 K MB spectra were largely devoid of any features, some spectra exhibited very low-intensity features that could be due to ferritins. The intensity of these features represented ~5% or less of total cellular iron. Such features had characteristics (at 5 K and 0.05 T) of either ferritin-associated iron or high-spin Fe^{III} heme or nonheme centers; these possibilities could not be distinguished. However, similar features were evident in spectra of samples in which FtnA had been deleted, in which case the features could not have originated from that ferritin. Also, EPR spectra of packed *E. coli* cells exhibited three low-field signals arising from mononuclear S = ½ Fe^{III} hemes and nonheme species. Such spin systems could have given rise to the MB baseline features. The 100 K high-temperature MB spectra of Δ*ftnA* cells exhibited similar magnetic features as at 5 K (but with reduced intensity). Collectively, our results demonstrate that no more than half of these minor MB features, barely distinguishable from baseline, could have arisen from FtnA-bound iron.

Evolution of respiratory shields as a strategy for dealing with O_2 and iron

Chemiosmotic coupling is as ancient a process as transcription and translation, and it is universally employed to generate energy in living systems (46). We propose that this process has important consequences for iron metabolism. Prior to the dramatic increase in atmospheric O_2 due to the evolution of photosynthetic organisms, early prokaryotes used molecules other than O_2 as terminal electron acceptors in chemiosmotic coupling. During that era, aqueous Fe^{II} dominated the environment, so these ancestral cells imported Fe^{II} and trafficked these ions through the cytosol for use in ISC assembly. This was followed by installation into various proteins, including nonoxygenic respiratory complexes located on the periplasmic membrane. Once O_2 appeared in the environment, it replaced these other molecules as the terminal electron acceptor in chemiosmotic energy coupling. This boosted the thermodynamics of the process such that more ATP could be generated per electron transferred. However, it also had negative consequences for iron trafficking and ROS damage.

We hypothesize that the newly evolved OXPHOS process provided a "respiratory shield" for these early prokaryotes. Such a shield is not a new concept; previous studies have provided evidence for it in aerobic bacteria. *Azotobacter vinelandii* uses a respiratory shield to protect nitrogenase, an extremely O_2-sensitive enzyme (47). In fact, the nitrogenase iron protein remains active when expressed in the mitochondrial matrix of yeast (48), which should be encapsulated by a respiratory shield on the inner membrane.

We hypothesize that during early stages of evolution, the shield maintained the cytosol at low O_2 concentrations as the pressure in the atmosphere increased. This allowed cytosolic Fe^{II} ions to continue to be used in trafficking because such ions were shielded from oxidation to the poorly soluble Fe^{III} state. For this reason, hexaqua Fe^{III} complexes could not be used in iron trafficking. Maintaining the respiratory shield simply required that the organisms metabolize nutrients fast enough to generate a rapid flow of electrons into the respiratory complexes, which in turn reduced O_2 fast enough to limit its diffusion into the cytosol.

Respiratory shields provide "safe spaces" for O_2-sensitive biochemistry in aerobic prokaryotes and mitochondria

At a later stage in evolution, an ancestor of α-proteobacteria was engulfed by a proto-eukaryotic host, culminating in a symbiotic relationship in which mitochondria provided chemical energy to the host via OXPHOS (49). Mitochondria and their bacterial ancestors share similar iron-rich respiration-related proteins as well as a suite of proteins involved in ISC biosynthesis (50, 51).

We report here that the iron content of *E. coli* and mitochondria are remarkably similar, at least at the coarse-grain level accessible by our methods. We recently proposed that the mitochondrial matrix in healthy eukaryotic cells is microaerobic and that this provides a safe space for O_2-sensitive enzymes (41, 42). This is especially important for ISC biosynthesis, an O_2-sensitive process that occurs in the matrix. The matrix contains a pool of labile LMM NHHS Fe^{II} (called Fe_{580}) that gives rise to a quadrupole doublet in MB spectra (Fig. S4, *blue line*) (52). Fe_{580} in mitochondria and Fe_{500} in *E. coli* may both serve as feedstock for ISC biosynthesis and possibly for the iron insertion step of heme biosynthesis. Although the two LMM complexes have different names, we cannot exclude the possibility that they are the same complex. Isolated mitochondria also exhibit an ISC doublet (Fig. S4, *green line*) with parameters that are nearly identical to those of the ISC doublet in *E. coli* spectra.

Previous results from the Lindahl laboratory (42, 52) suggest that nanoparticles form in mitochondria when O_2 penetrates the matrix and reacts with Fe_{580}, as illustrated in Fig. 6 (*top*). O_2 penetrates ISC-deficient mitochondria because the respiratory shield is disabled. Under these conditions, the respiratory complexes are probably not fully loaded with ISCs and heme centers, and are thus unable to transfer sufficient electrons from the tricarboxylic acid cycle to cytochrome *c* oxidase and then to O_2. In healthy mitochondria, more of the O_2 that diffuses to the IM is reduced to H_2O so that this diatomic molecule cannot overwhelm the matrix. We now propose an equivalent mechanism in *E. coli* and other aerobic bacteria (Fig. 6, *bottom*). Electrons generated by the metabolic activity of the cell are delivered to the inner membrane complexes and eventually to cytochrome *c* oxidase. This rapidly reduces some of the O_2 that would otherwise diffuse into the cytosol. When the metabolic activity of the organism declines, as when cells transition to stationary phase, more O_2 penetrates the cytosol, where it can react with Fe_{500} to form nanoparticles. The content and O_2-associated reactivity of iron in mitochondria and bacteria are similar largely because both have respiratory shields.

Examining the iron content of all bacteria is not possible, but published MB spectra of various bacteria support a common iron content, at least at the coarse-grain level of our analysis. The MB spectra of *Pseudomonas aeruginosa* whole cells (harvested after 44 h of growth) exhibit the same features as we observed for *E. coli* and mitochondria, namely a magnetically ordered Fe^{III} doublet, an ISC doublet, and a NHHS Fe^{II} doublet (53). The 82 K MB spectrum of *Proteus mirabilis* consists of a broad magnetically ordered Fe^{III} doublet as well as a NHHS Fe^{II} doublet (54). MB spectra of *Erwinia chrysanthemi* (grown on glucose, harvested in stationary state) exhibit a magnetically ordered Fe^{III} doublet and a NHHS Fe^{II} doublet (55).

To provide further evidence for a common (coarse-grain) iron content in prokaryotes, we examined the MB spectrum of Gram-positive *Bacillus subtilis* harvested under exponential growth conditions. As predicted, the spectrum (Fig. S7) was similar to those of *E. coli* and mitochondria. The MB spectrum of *B. subtilis* exhibited more magnetic iron than in *E. coli* or mitochondria, but the difference is only one of degree. Viewed collectively, these results provide strong support for a common (coarse-grain) iron content in aerobic prokaryotes and mitochondria.

The respiratory shield, NHHS Fe^{II}_{LMM}, and nanoparticles might collectively serve to regulate and store iron in prokaryotes

Eukaryotes protect against Fenton chemistry by minimizing the concentration of Fe^{II} in the cytosol and by storing excess iron in ferritin (or in vacuoles, for fungi and plants). It was

reasonable to assume that *E. coli* and other prokaryotes use the same strategies. However, this does not appear to be the case. As strange as it sounds, metabolically active aerobic *E. coli* simply do *not* store much iron, certainly not in ferritin cores. Under lower O_2 conditions, *E. coli* does not minimize the concentration of labile Fe^{II} species in the cytosol; in fact, they might store iron as labile Fe^{II}. Metabolically active *E. coli* avoid Fenton chemistry by reducing the amount of O_2 that diffuses into the cytosol via the respiratory shield. Metabolically dormant *E. coli* store iron mainly as Fe^{III} oxyhydroxide nanoparticles. Although we have not determined whether *E. coli* can utilize such iron when they reactivate metabolically, yeast cells are able to do this (56). The implication is that ferritins play more specialized and limited roles in storing iron in *E. coli* cells than has been considered previously.

The love-hate relationship of cells with O_2 involves respiratory shields and antioxidant swords

The concentration of O_2 in the mitochondrial matrix, *E. coli*, and other aerobic prokaryotes has not been measured directly, so estimates vary. Unden and co-workers (57) measured O_2 consumption rates of bacterial cultures and calculated O_2 diffusion rates. They concluded that the O_2 concentration in the cytosol of bacteria is essentially the same as in external aerobic environments. This conclusion implies that the respiratory shield is weak and ineffective, and it supports the view that a multilayered antioxidant system (involving SOD, catalases, peroxidases, etc.) is continuously and vigorously fighting against ROS damage in healthy metabolically active cells and rapidly repairing any damage that occurs. We stress that the respiratory shield is not completely effective in preventing O_2 from entering the cytosol or matrix, and we recognize the critical importance of the antioxidant system. These protected spaces certainly contain some O_2 and O_2-derived ROS, as evidenced by enzymes (*e.g.* dioxygenases, superoxide dismutases, and FNR) that are in these spaces and use O_2 as substrates. However, we suggest that cells use both a respiratory "shield" and an antioxidant "sword" in their battle with O_2. By locating the respiratory shield near their peripheries, cells reap the energetic benefits of using O_2 in OXPHOS while at the same time minimizing exposure to O_2-sensitive cytosolic species. We look forward to probing further this intriguing love-hate relationship between aerobic cells and the molecule that they so desperately need but also the one that poses an existential threat to their very survival.

Experimental procedures

Construction of cell strains

The Δ*fur::kan*^{R}, Δ*ftnA::kan*^{R}, and Δ*bfr::kan*^{R}Δ*dps::cm*^{R} mutations were constructed by replacing the indicated open reading frames in strain DY330 with the kanamycin resistance cassette (*kan*^{R}) from pKD4 or the chloramphenicol resistance cassette (*cm*^{R}) from pKD3 using the λ RED system as described (58). Mutations were moved by P1 transduction into the MG1655 or other strain backgrounds. MG1655 Δ*bfr* was generated by removal of the *kan*^{R} cassette from the MG1655 Δ*bfr::kan*^{R} strain using the pCP20 plasmid as described (58).

Cells and growth

A single colony of each strain was inoculated into 50 ml of M9 minimal medium containing 0.2% (w/v) glucose. Cultures were incubated overnight at 37 °C and ~200 rpm. Grown cultures were used to inoculate 1–2 liters of the same medium but supplemented with 1, 10, or 100 μM $^{57}Fe^{III}$ citrate. For exponential growths, cells were harvested at A_{600} = 0.5–0.8. Stationary-phase samples were harvested at A_{600} ~1.2.

The same procedure was used for cells grown on acetate except that the medium contained 0.4% (w/v) sodium acetate rather than glucose. For MB or EPR samples, harvested cells were centrifuged and washed with 50 ml of 50 mM EDTA, 100 mM sodium oxalate, 100 mM NaCl, and 10 mM KCl. Washed cells were packed into either MB cups or EPR tubes and then frozen in liquid N_2. WT *B. subtilis* cells (a generous gift of Jennifer K Herman, Texas A&M University (TAMU)) were grown in glucose-containing M9 medium under aerobic conditions and supplemented with 100 μM ^{57}Fe citrate. Cells were harvested during exponential phase (A_{600} = 0.6) and a MB sample was prepared as above.

For experiments involving cyanide, WT cells were inoculated into 2 liters of minimal medium containing glucose and 100 μM iron citrate in a 2.8-liter baffled flask and incubated as above. Half of the cells were harvested during exponential phase (A_{600} ~0.65) and used to prepare a MB sample. The other half was incubated with 3.0 mM KCN (final concentration) and then used to prepare an MB sample after 1.5 h of incubation. Metal analysis and LC-ICP-MS experiments were performed essentially as described (42, 44) using MB samples after spectra had been collected. For metal analyses, a packing efficiency of 0.7 volume of cells/volume of packed wet cells was assumed, as was a density of 1.1 g/ml.

For LC-ICP-MS studies, samples (~800 μl) were thawed in the glove box and suspended in a 15-ml Falcon tube containing 5.0 ml of 20 mM ammonium bicarbonate, pH 8.5, ~100 mg of lysozyme (Sigma-Aldrich), and 2.0 ml of 0.1-mm diameter acid-washed glass beads (Sigma-Aldrich). The suspension was vortexed for 5 min and then placed in an ice bath for 5 min. This process was repeated twice. The lysate was then centrifuged for 15 min at 12,000 × *g* (Sorvall Evolution RC centrifuge, GSA rotor). One ml of supernatant was mixed with 1.0 ml of 2% (v/v) Triton X-100 (Sigma-Aldrich), affording a 1% final concentration of Triton. The solution was vortexed for 30 min. (The remaining supernatant was frozen at −80 °C.) The Triton-containing lysate was spun at 12,000 × *g* for 15 min. The resulting supernatant (~2 ml) was passed through an Ultracel 10-kDa ultrafiltration membrane using a stirred cell concentrator (Amicon, Millipore). Three hundred microliters of each FTS was injected onto two Superdex Peptide 10/300 GL (GE Healthcare) columns connected in series, equilibrated in 20 mM ammonium bicarbonate, pH 8.5.

Mössbauer spectra were collected on an MS4 WRC or LHe6T spectrometer (SEE Co., Edina, MN). Spectra were simulated with WMOSS software, and calibrated at room temperature with α-iron foil. EPR spectra were recorded using an X-band Elexsys E500 spectrometer (Bruker Biospin Corp., Billerica, MA). EPR spectra were simulated using SpinCount.

Author contributions—J. D. W., F. W. O., and P. A. L. conceptualization; J. D. W., F. W. O., and P. A. L. formal analysis; J. D. W., N. B., and N. D. investigation; J. D. W., F. W. O., and P. A. L. writing-review and editing; N. D. methodology; F. W. O. and P. A. L. supervision; F. W. O. and P. A. L. resources; F. W. O. and P. A. L. funding acquisition; P. A. L. writing-original draft.

References

1. Mettert, E. L., and Kiley, P. J. (2015) How Is Fe-S Cluster Formation Regulated? *Annu. Rev. Microbiol.* **69,** 505–526 CrossRef Medline
2. Rouault, T. A., and Tong, W. H. (2005) Iron–sulphur cluster biogenesis and mitochondrial iron homeostasis. *Nat. Rev.* **6,** 345–351 CrossRef Medline
3. Braymer, J. J., and Lill, R. (2017) Iron-sulfur cluster biogenesis and trafficking in mitochondria. *J. Biol. Chem.* **292,** 12754–12763 CrossRef Medline
4. Outten, F. W., and Theil, E. C. (2009) Iron-based redox switches in biology. *Antioxid. Redox Signal.* **11,** 1029–1046 CrossRef Medline
5. Gütlich, P., Bill, E., and Trautwein, A. X. (2011) *Mössbauer Spectroscopy and Transition Metal Chemistry*, Springer, New York
6. Münck, E. (2000) Aspects of ^{57}Fe Mössbauer spectroscopy. In *Physical Methods in Bioinorganic Chemistry: Spectroscopy and Magnetism* (Que, L., Jr., ed) pp. 287–320, University Science Books, Sausalito, CA
7. Papaefthymiou, G. C. (2010) The Mössbauer and magnetic properties of ferritin cores. *Biochim. Biophys. Acta* **1800,** 886–897 CrossRef Medline
8. Bradley, J. M., Le Brun, N. E., and Moore, G. R. (2016) Ferritins: furnishing proteins with iron. *J. Biol. Inorg. Chem.* **21,** 13–28 CrossRef Medline
9. de Castro Ferreira, I. G., Rodrigues, M. M., da Silva Neto, J. F., Mazzon, R. R., and do Valle Marques, M. (2016) Role and regulation of ferritin-like proteins in iron homeostasis and oxidative stress survival of *Caulobacter crescentus*. *Biometals* **29,** 851–862 CrossRef Medline
10. Bauminger, E. R., Cohen, S. G., Dickson, D. P. E., Levy, A., Ofer, S., and Yariv, J. (1980) Mössbauer spectroscopy of *Escherichia coli* and its iron storage protein. *Biochim. Biophys. Acta* **623,** 237–242 CrossRef Medline
11. Matzanke, B. F., Müller, G. I., Bill, E., and Trautwein, A. X. (1989) Iron metabolism of *Escherichia coli* studied by Mössbauer spectroscopy and biochemical methods. *Eur. J. Biochem.* **183,** 371–379 CrossRef Medline
12. Hudson, A. J., Andrews, S. C., Hawkins, C., Williams, J. M., Izuhara, M., Meldrum, F. C., Mann, S., Harrison, P. M., and Guest, J. R. (1993) Overproduction, purification and characterization of the *Escherichia coli* ferritin. *Eur. J. Biochem.* **218,** 985–995 CrossRef Medline
13. Abdul-Tehrani, H., Hudson, A. J., Chang, Y. S., Timms, A. R., Hawkins, C., Williams, J. M., Harrison, P. M., Guest, J. R., and Andrews, S. C. (1999) Ferritin mutants of *Escherichia coli* are iron deficient and growth impaired, and fur mutants are iron deficient. *J. Bacteriol.* **181,** 1415–1428 Medline
14. Fontecave, M., and Pierre, J. L. (1991) Iron metabolism: the low-molecular-mass iron pool. *Biol. Met.* **4,** 133–135 CrossRef Medline
15. Böhnke, R., and Matzanke, B. F. (1995) The mobile ferrous iron pool in *E. coli* is bound to a phosphorylated sugar derivative. *Biometals* **8,** 223–230 Medline
16. Woodmansee, A. N., and Imlay, J. A. (2002) Quantitation of intracellular free iron by electron paramagnetic resonance spectroscopy. *Methods Enzymol.* **349,** 3–9 CrossRef Medline
17. Ma, Z., Faulkner, M. J., and Helmann, J. D. (2012) Origins of specificity and cross-talk in metal ion sensing by *Bacillus subtilis* Fur. *Mol. Microbiol.* **86,** 1144–1155 CrossRef Medline
18. Keyer, K., and Imlay, J. A. (1996) Superoxide accelerates DNA damage by elevating free-iron levels. *Proc. Natl. Acad. Sci. U.S.A.* **93,** 13635–13640 CrossRef Medline
19. Bagg, A., and Neilands, J. B. (1987) Ferric uptake regulation protein acts as a repressor, employing iron(II) as a cofactor to bind the operator of an iron transport operon in *Escherichia coli*. *Biochemistry* **26,** 5471–5477 CrossRef Medline
20. Beauchene, N. A., Mettert, E. L., Moore, L. J., Keleş, S., Willey, E. R., and Kiley, P. J. (2017) O_2 availability impacts iron homeostasis in *Escherichia coli*. *Proc. Natl. Acad. Sci. U.S.A.* **114,** 12261–12266 CrossRef Medline
21. Woodmansee, A. N., and Imlay, J. A. (2002) Reduced flavins promote oxidative DNA damage in non-respiring *Escherichia coli* by delivering electrons to intracellular free iron. *J. Biol. Chem.* **277,** 34055–34066 CrossRef Medline
22. Hamed, M. Y. (1993) Binding of the ferric uptake regulation repressor protein (Fur) to Mn(II), Fe(II), Co(II), and Cu(II) ions as co-repressors: electronic absorption, equilibrium, and ^{57}Fe Mössbauer studies. *J. Inorg. Biochem.* **50,** 193–210 CrossRef Medline
23. Hohle, T. H., and O'Brian, M. R. (2016) Metal-specific control of gene expression mediated by *Bradyrhizobium japonicum* Mur and *Escherichia coli* Fur is determined by the cellular context. *Mol. Microbiol.* **101,** 152–166 CrossRef Medline
24. Fillat, M. F. (2014) The FUR (ferric uptake regulator) superfamily: diversity and versatility of key transcriptional regulators. *Arch. Biochem. Biophys.* **546,** 41–52 CrossRef Medline
25. McHugh, J. P., Rodríguez-Quiñones, R., Abdul-Tehrani, H., Svistunenko, D. A., Poole, R. K., Cooper, C. E., and Andrews, S. C. (2003) Global iron-dependent gene regulation in *Escherichia coli*: a new mechanism for iron homeostasis. *J. Biol. Chem.* **278,** 29478–29486 CrossRef Medline
26. Lemercier, G., Mulliez, E., Brouca-Cabarrecq, C., Dahan, F., and Tuchagues, J. P. (2004) Iron(II) carboxylate complexes based on a tetraimidazole ligand as models of the photosynthetic non-heme ferrous sites: synthesis, crystal structure, and Mössbauer and magnetic studies. *Inorg. Chem.* **43,** 2105–2113 CrossRef Medline
27. Jacques, J.-F., Jang, S. J., Prévost, K., Desnoyers, G., Desmarais, M., Imlay, J., and Massé, E. (2006) RyhB small RNA modulates the free intracellular iron pool and is essential for normal growth during iron limitation in *Escherichia coli*. *Mol. Microbiol.* **62,** 1181–1190 CrossRef Medline
28. Mills, S. A., and Marletta, M. A. (2005) Metal binding characteristics and role of iron oxidation in the ferric uptake regulator from *Escherichia coli*. *Biochemistry* **44,** 13553–13559 CrossRef Medline
29. Lau, C. K. Y., Krewulak, K. D., and Vogel, H. J. (2016) Bacterial ferrous ion transport: the Feo system. *FEMS Microbiol. Rev.* **40,** 273–298 CrossRef Medline
30. Kiley, P. J., and Beinert, H. (1998) Oxygen sensing by the global regulator, FNR: the role of the iron-sulfur cluster. *FEMS Microbiol. Rev.* **22,** 341–352 CrossRef Medline
31. Hristova, D., Wu, C. H., Jiang, W., Krebs, C., and Stubbe, J. (2008) Importance of the maintenance pathway in the regulation of the activity of the *Escherichia coli* ribonucleotide reductase. *Biochemistry* **47,** 3989–3999 CrossRef Medline
32. Beilschmidt, L. K., Ollagnier de Choudens, S., Fournier, M., Sanakis, I., Hograindleur, M. A., Clémancey, M., Blondin, G., Schmucker, S., Eisenmann, A., Weiss, A., Koebel, P., Messaddeq, N., Puccio, H., and Martelli, A. (2017) ISCA1 is essential for mitochondrial Fe_4S_4 biogenesis *in vivo*. *Nat. Commun.* **8,** 15124 CrossRef Medline
33. Outten, C. E., O'Halloran, T. V. (2001) Femtomolar sensitivity of metalloregulatory proteins controlling zinc homeostasis. *Science* **292,** 2488–2492 CrossRef Medline
34. Paalme, T., Elken, R., Kahru, A., Vanatalu, K., and Vilu, R. (1997) The growth rate control in *Escherichia coli* at near to maximum growth rates: the A-stat approach. *Antonie Van Leeuwenhoek* **71,** 217–230 CrossRef Medline
35. Park, J., McCormick, S. P., Chakrabarti, M., and Lindahl, P. A. (2013) The lack of synchronization between iron uptake and cell growth leads to iron overload in *Saccharomyces cerevisiae* during postexponential growth modes. *Biochemistry* **52,** 9413–9425 CrossRef Medline
36. Miao, R., Kim, H., Koppolu, U. M. K., Ellis, E. A., Scott, R. A., and Lindahl, P. A. (2009) Biophysical characterization of the iron in mitochondria from Atm1p-depleted *Saccharomyces cerevisiae*. *Biochemistry* **48,** 9556–9568 CrossRef Medline
37. Popescu, C. V., Bates, D. M., Beinert, H., Münck, E., and Kiley, P. J. (1998) Mössbauer spectroscopy as a tool for the study of activation/inactivation of the transcription regulator FNR in whole cells of *Escherichia coli*. *Proc. Natl. Acad. Sci. U.S.A.* **95,** 13431–13435 CrossRef Medline
38. Miao, R., Holmes-Hampton, G. P., and Lindahl, P. A. (2011) Biophysical investigation of the iron in Aft1–1(up) and Gal-YAH1 *Saccharomyces cerevisiae*. *Biochemistry* **50,** 2660–2671 Medline

39. Benda, R., Tse Sum Bui, B., Schünemann, V., Florentin, D., Marquet, A., and Trautwein, A. X. (2002) Iron-sulfur clusters of biotin synthase *in vivo*: a Mössbauer study. *Biochemistry* **41,** 15000–15006 CrossRef Medline
40. Jhurry, N. D., Chakrabarti, M., McCormick, S. P., Holmes-Hampton, G. P., and Lindahl, P. A. (2012) Biophysical investigation of the ironome of human Jurkat cells and mitochondria. *Biochemistry* **51,** 5276–5284 CrossRef Medline
41. Wofford, J. D., and Lindahl, P. A. (2015) Mitochondrial iron-sulfur-cluster activity and cytosolic iron regulate iron traffic in *Saccharomyces cerevisiae*. *J. Biol. Chem.* **290,** 26968–26977 CrossRef Medline
42. Moore, M. J., Wofford, J. D., Dancis, A., and Lindahl, P. A. (2018) Recovery of mrs3Δmrs4Δ *Saccharomyces cerevisiae* cells under iron sufficient conditions and the role of Fe_{580}. *Biochemistry* **57,** 672–683 CrossRef Medline
43. Waldron, K. J., Rutherford, J. C., Ford, D., and Robinson, N. J. (2009) Metalloproteins and metal sensing. *Nature* **460,** 823–830 CrossRef Medline
44. Dziuba, N., Hardy, J., and Lindahl, P. A. (2018) Low-molecular-mass iron in healthy blood plasma is not predominately ferric citrate. *Metallomics* **10,** 802–817 CrossRef Medline
45. Escolar, L., Pérez-Martín, J., and De Lorenzo, V. (1999) Opening the iron box: transcriptional metalloregulation by the fur protein. *J. Bacteriol.* **181,** 6223–6229 Medline
46. Lane, N. (2014) Bioenergetic constraints on the evolution of complex life. *Cold Spring Harb. Perspect. Biol.* **6,** a015982 CrossRef Medline
47. Poole, R. K. (1994) Oxygen reactions with bacterial oxidases and globins: binding, reduction and regulation. *Antonie Van Leeuwenhoek* **65,** 289–310 CrossRef Medline
48. López-Torrejón, G., Jiménez-Vicente, E., Buesa, J. M., Hernandez, J. A., Verma, H. K., and Rubio, L. M. (2016) Expression of a functional oxygen-labile nitrogenase component in the mitochondrial matrix of aerobically grown yeast. *Nat. Commun.* **7,** 11426 CrossRef Medline
49. Carvalho, D. S., Andrade, R. F. S., Pinho, S. T. R., Góes-Neto, A., Lobão, T. C. P., Bomfim, G. C., and El-Hani, C. N. (2015) What are the evolutionary origins of mitochondria? A complex network approach. *PLoS One* **10,** e0134988 CrossRef Medline
50. Tachezy, J., Sánchez, L. B., and Müller, M. (2001) Mitochondrial type iron-sulfur cluster assembly in the amitochondriate eukaryotes *Trichomonas vaginalis* and *Giardia intestinalis*, as indicated by the phylogeny of IscS. *Mol. Biol. Evol.* **18,** 1919–1928 CrossRef Medline
51. Al-Attar, S., and de Vries, S. (2013) Energy transduction by respiratory metallo-enzymes: from molecular mechanism to cell physiology. *Coord. Chem. Rev.* **257,** 64–80 CrossRef
52. McCormick, S. P., Moore, M. J., and Lindahl, P. A. (2015) Detection of labile low-molecular-mass transition metal complexes in mitochondria. *Biochemistry* **54,** 3442–3453 CrossRef Medline
53. Kadir, F. H., Read, N. M., Dickson, D. P., Greenwood, C., Thompson, A., and Moore, G. R. (1991) Mössbauer spectroscopic studies of iron in *Pseudomonas ariginosa*. *J. Inorg. Biochem.* **43,** 753–758 CrossRef Medline
54. Dickson, D. P. E., and Rottem, S. (1979) Mössbauer spectroscopic studies of iron in *Proteus mirabilis*. *Eur. J. Biochem.* **101,** 291–295 CrossRef Medline
55. Boughammoura, A., Matzanke, B. F., Böttger, L., Reverchon, S., Lesuisse, E., Expert, D., and Franza, T. (2008) Differential role of ferritins in iron metabolism and virulence of the plant-pathogenic bacterium *Erwinia chrysanthemi 3937*. *J. Bacteriol.* **190,** 1518–1530 CrossRef Medline
56. Wofford, J. D., Park, J., McCormick, S. P., Chakrabarti, M., and Lindahl, P. A. (2016) Ferric ions accumulate in the walls of metabolically inactivating *Saccharomyces cerevisiae* cells and are reductively mobilized during reactivation. *Metallomics* **8,** 692–708 CrossRef Medline
57. Arras, T., Schirawski, J., and Unden, G. (1998) Availability of O_2 as a substrate in the cytoplasm of bacteria under aerobic and microaerobic conditions. *J. Bacteriol.* **180,** 2133–2136 Medline
58. Datsenko, K. A., and Wanner, B. L. (2000) One-step inactivation of chromosomal genes in *Escherichia coli* K-12 using PCR products. *Proc. Natl. Acad. Sci. U.S.A.* **97,** 6640–6645 CrossRef Medline
59. Reisner, E., Telser, J., and Lippard, S. J. (2007) A planar carboxylate-rich tetrairon(II) complex and its conversion to linear triiron(II) and paddlewheel diiron(II) complexes. *Inorg. Chem.* **46,** 10754–10770 CrossRef Medline
60. Reiff, W. M., Frankel, R. B., and Abeledo, C. R. (1973) Orbital ground state inversion in $[Fe(H_2O)_6](ClO_4)_2$. *Chem. Phys. Lett.* **22,** 124–126 CrossRef
61. Clemente-Juan, J. M., Mackiewicz, C., Verelst, M., Dahan, F., Bousseksou, A., Sanakis, Y., and Tuchagues, J. P. (2002) Synthesis, structure, and magnetic properties of tetranuclear cubane-like and chain-like iron(II) complexes based on the N_4O pentadentate dinucleating ligand 1,5-Bis[2-pyridylmethyl)amino]pentan-3-ol. *Inorg. Chem.* **41,** 1478–1491 CrossRef Medline

Evidence that a respiratory shield in *Escherichia coli* protects a low-molecular-mass Fe^{II} pool from O_2-dependent oxidation

Joshua D. Wofford, Naimah Bolaji, Nathaniel Dziuba, F. Wayne Outten and Paul A. Lindahl

J. Biol. Chem. 2019, 294:50-62.
doi: 10.1074/jbc.RA118.005233 originally published online October 18, 2018